**RESEARCH PAPER**

# Overexpression of the chloroplastic 2-oxoglutarate/malate transporter disturbs carbon and nitrogen homeostasis in rice

**Shirin Zamani-Nour**[1,*], **Hsiang-Chun Lin**[2,*], **Berkley J. Walker**[1,iD], **Tabea Mettler-Altmann**[1,iD],
**Roxana Khoshravesh**[3], **Shanta Karki**[4], **Efren Bagunu**[2], **Tammy L. Sage**[3,iD], **W. Paul Quick**[2,5] and
**Andreas P.M. Weber**[1,†,iD]

[1] Institute of Plant Biochemistry, Cluster of Excellence on Plant Science (CEPLAS), Heinrich-Heine University, Universitätsstrasse 1, D-40225 Düsseldorf, Germany
[2] International Rice Research Institute, Los Baños, Laguna, Philippines
[3] Department of Ecology and Evolutionary Biology, University of Toronto, 25 Willcocks Street, Toronto, Ontario M5S3B2, Canada
[4] National Center for Fruit Development, Kirtipur, Kathmandu, Nepal
[5] Department of Animal and Plant Sciences, University of Sheffield, Sheffield S10 2TN, UK

* These authors contributed equally to this work.
† Correspondence: andreas.weber@uni-duesseldorf.de

## Abstract

**The chloroplastic 2-oxaloacetate (OAA)/malate transporter (OMT1 or DiT1) takes part in the malate valve that protects chloroplasts from excessive redox poise through export of malate and import of OAA. Together with the glutamate/malate transporter (DCT1 or DiT2), it connects carbon with nitrogen assimilation, by providing 2-oxoglutarate for the GS/GOGAT (glutamine synthetase/glutamate synthase) reaction and exporting glutamate to the cytoplasm. OMT1 further plays a prominent role in $C_4$ photosynthesis: OAA resulting from phosphoenolpyruvate carboxylation is imported into the chloroplast, reduced to malate by plastidic NADP-malate dehydrogenase, and then exported for transport to bundle sheath cells. Both transport steps are catalyzed by OMT1, at the rate of net carbon assimilation. To engineer $C_4$ photosynthesis into $C_3$ crops, OMT1 must be expressed in high amounts on top of core $C_4$ metabolic enzymes. We report here high-level expression of *ZmOMT1* from maize in rice (*Oryza sativa* ssp. *indica* IR64). Increased activity of the transporter in transgenic rice was confirmed by reconstitution of transporter activity into proteoliposomes. Unexpectedly, overexpression of *ZmOMT1* in rice negatively affected growth, $CO_2$ assimilation rate, total free amino acid content, tricarboxylic acid cycle metabolites, as well as sucrose and starch contents. Accumulation of high amounts of aspartate and the impaired growth phenotype of OMT1 rice lines could be suppressed by simultaneous overexpression of *ZmDiT2*. Implications for engineering $C_4$ rice are discussed.**

**Keywords:** Carbon and nitrogen assimilation, $C_4$ rice, gas exchange, glutamate/malate transporter, oxaloacetate/malate transporter, photosynthesis.

## Introduction

Population growth, climate change, and lack of arable land are causing greater dependence on crop yield improvement. However, crop demand is already outpacing the yield gains achieved by conventional breeding and, hence, stepwise changes in crop yield are needed (Kromdijk and Long, 2016). Rice (*Oryza sativa* L.) is a $C_3$ grass and one of the top three staple crops in the world. Its highest consumption is in Asia (Muthayya *et al.*, 2014) where 60% of the world population exists (Bai *et al.*, 2018), with the highest and lowest rates of poverty and income, respectively (FAO, 2017). Therefore, boosting rice yield and performance is an important goal for improving the quality of life for a large share of the global population. Engineering the $C_3$ crop rice to perform $C_4$ photosynthesis would greatly improve rice productivity by up to 50% per year (Wang *et al.*, 2016), through maximizing the conversion of the captured solar energy into chemical energy and biomass (Hibberd *et al.*, 2008).

$C_3$ photosynthesis performs both initial carbon fixation and Calvin–Benson cycle reactions in the mesophyll. In $C_4$ photosynthesis, initial carbon fixation and the Calvin–Benson cycle are carried out separately in the mesophyll and one or more layers of sheath cells (bundle and/or mestome sheath) surrounding the vascular tissue, respectively. This spatial separation concentrates $CO_2$ around the enzyme Rubisco, thereby reducing Rubisco oxygenase activity and the subsequent loss of energy and previously fixed $CO_2$ during photorespiration (Sage *et al.*, 2012). Suppressing the energy and $CO_2$ loss from photorespiration leads to greater plant biomass, and nitrogen- and water-use efficiency (Ghannoum *et al.*, 2011). $C_4$ photosynthesis also represents an adaptation for coping with stressful conditions, such as drought, high temperature, and light intensity (Edwards *et al.*, 2010).

Chloroplasts with their double-envelope membrane and internal compartments play a critical role in carbon fixation and photosynthesis. Since biological membranes form barriers for the diffusion of hydrophilic metabolites, membrane transporters are required for the selective flux of polar molecules and metabolites across the chloroplast membrane (Haferkamp and Linka, 2012). One of the transporters that resides in the plastid inner envelope membrane is known as oxaloacetate (OAA)/malate transporter 1 (OMT1) or dicarboxylate transporter 1 (DiT1). The gene is expressed ubiquitously in roots, stems, leaves, florescences, and siliques of mature Arabidopsis plants (Taniguchi *et al.*, 2002), and the protein is an OAA/malate antiporter with 12 α-helical transmembrane domains. OMT1/DIT1 functions to transport substrates according to the electrochemical gradient generated by solutes inside and outside the chloroplast membrane (Weber *et al.*, 1995). This transporter, in concert with malate dehydrogenase (MDH; plastidic and cytosolic isoforms), forms the malate shunt that plays a key role in exporting excess reducing compounds from the chloroplast, to protect PSII, and to balance stromal redox potential (Selinski and Scheibe, 2019).

Redox balancing through the OMT1/DiT1-mediated malate valve is expected to be more beneficial when photorespiratory rates are increased, since higher relative rates of photorespiration increase the ATP/NAPDH demand of central metabolism, resulting in an excess of reduced NADPH in the plastid (Kramer and Evans, 2011; Walker *et al.*, 2014). The malate valve can serve to oxidize the over-reduced NADPH pool to regenerate oxidized $NADP^+$ carriers that are needed to maintain electron transport. The NADH generated in the cytosol from the malate valve activity is consumed in other reactions such as nitrate reduction. The resulting nitrite is imported into chloroplasts where it is further reduced to ammonia that is subsequently assimilated into glutamate by the GS/GOGAT (glutamine synthase/glutamate synthase) pathway (Tobin and Yamaya, 2001; Selinski and Scheibe, 2019). Glutamate itself is a building block for the biosynthesis of many amino acids (Forde and Lea, 2007). OMT1, jointly with the DiT2/DCT1 transporter (a glutamate/malate transporter), therefore connects carbon and nitrogen metabolism while equilibrating the ATP/NADPH ratio in chloroplast stroma (Taniguchi *et al.*, 2002; Kinoshita *et al.*, 2011; Taniguchi and Miyake, 2012). The strong, visibly perturbed phenotypes of *omt1* mutants in Arabidopsis (Kinoshita *et al.*, 2011) and in tobacco (Schneidereit *et al.*, 2006) confirm its crucial role in carbon and nitrogen assimilation pathways as well as in plant growth and development.

OMT1 also plays an important role in $C_4$ photosynthesis. The transporter imports OAA that is formed by cytosolic phosphoenolpyruvate carboxylase (PEPC) into mesophyll cell chloroplasts where it is reduced to malate by NADP-MDH. OMT1 also facilitates the export of malate to the cytosol. These transport steps occur at the same rate as $CO_2$ assimilation and thus, for engineering $C_4$ photosynthesis into $C_3$ crops such as rice, high expression and activity of OMT1 are required. In this study, as part of the effort to engineer $C_4$ rice, we introduced the *ZmOMT1* gene from $C_4$ maize into $C_3$ rice to achieve sufficiently highly transport capacity for OAA and malate across the chloroplast envelope. Additionally, since $C_4$ photosynthesis requires a complex array of biochemical and anatomical components, we investigate whether *ZmOMT1* expression triggers anatomical features found in $C_4$ plants, which could further aid continued $C_4$ engineering efforts.

## Materials and methods

*Rice transformation and growth conditions*

To express maize *ZmOMT1* in rice mesophyll cells, we transferred the pSC110:*ZmOMT1*:AcV5 construct into *Oryza sativa* spp. *indica* cultivar IR64 (Mackill and Khush, 2018). The construct contains the full-length cDNA of the *ZmOMT1* gene (GRMZM2G383088) from maize (*Zea mays* var. B73) with a C-terminal AcV5 epitope tag, driven by the maize B73 mesophyll-specific *ZmPEPC* promoter (GRMZM2G083841; base pairs −1212 to +1) from the pSC110 vector (Supplementary Fig. 1A at *JXB* online). The forward and reverse primers given in Supplementary Table S1) were used to clone the coding sequence via the pENTR vector into the pSC110 expression vector utilizing the Gateway cloning system

(Thermo Fisher Scientific). The pSC110 vector was generated as previously described (Osborn *et al.*, 2017). The AcV5 epitope tag was placed downstream of the *ZmOMT1* coding sequence (CDS) for later detection of expressed protein using commercially available AcV5 antibody. The final construct was transferred into freshly harvested immature embryos 8–12 d after anthesis using an *Agrobacterium*-mediated transformation protocol as described in Yin *et al.* (2019). After 1 week of co-cultivation and following 5 d on non-selective medium, emerging resistant calli were selected with 30 mg l$^{-1}$ hygromycin B. The transgenic plants generated from hygromycin-resistant calli were transferred to Yoshida hydroponic solution (Yoshida *et al.*, 1972) for 2 weeks and then transplanted into 0.5 liter pots filled with soil. Plants were grown in a greenhouse at the International Rice Research Institute (IRRI, Los Baños, Philippines: 14°9'53.58"S 121°15'32.19"E). The average day/night temperatures were 35±3 °C and 28±3 °C, respectively. The average and maximum light intensities were 825 µmol photons m$^{-2}$ s$^{-1}$ and 2000 µmol photons m$^{-2}$ s$^{-1}$, respectively. Seeds of transgenic plants were germinated in distilled water for 1 week and transplanted into soil in 100 ml Rootrainers (http://rootrainers.co.uk/). After 2 weeks, plants were transplanted to 7 liter soil pots. Plants were grown at Heinrich-Heine University (HHU) Düsseldorf, Germany under semi-controlled greenhouse conditions (16 h day/8 h night and 25 °C). Assessment of leaf gas exchange, as well as metabolite, C:N ratio, total free amino acids, and transporter activity measurements were performed at HHU.

### PCR screening

Homozygous transgenic lines were screened by performing genomic PCR using the KAPA 3G plant PCR kit (Kapa Biosystem, USA). Leaves were harvested 7 d after transplanting plants into soil; scraped leaves were directly used as the template for PCR amplification of *ZmOMT1* in a 10 µl total volume employing the gene-specific primers given in Supplementary Table S1. PCR conditions were: 95 °C for 5 min, 32 cycles of 95 °C for 20 s, 60 °C for 15 s, and 72 °C for 30 s; and 72 °C for 1 min using the plasmid DNA as a positive control and non-transgenic rice leaf tissue or water as negative controls.

### Quantitative real-time PCR (qRT-PCR)

qRT-PCR was performed to quantify *OsOMT1* and *ZmOMT1* transcript expression levels in 8-week-old plants. Leaf RNA was extracted using a QIAGEN RNeasy Mini Kit from three biological replicates. Then one-step cDNA synthesis using LunaScript™ RT SuperMix Kit (NEB Biolabs, USA) was followed by total 20 µl volume master mix preparation (Luna® Universal qPCR Master Mix NEB Biolabs, USA). PCRs were performed in a 7500 Fast Real-Time PCR System (Invitrogen, USA), and guided using the primer pairs given in Supplementary Table S1. The PCR conditions were: 95 °C for 60 s, 40 cycles of 95 °C for 15 s, and 60 °C for 30 s, followed by the measurement of the melting curve after 40 cycles for primer specificity. The primer efficiency was calculated as described by Udvardi *et al.* (2008) using different dilutions of cDNA together with a highly stable housekeeping gene from rice, *OsEF-1a* (Os03g0177500) (Jain *et al.*, 2006). The mean normalized expression (MNE) for calculation of average CT was used as described by Simon (2003).

### Reverse transcription PCR (RT–PCR)

To detect the *ZmOMT1* and *ZmDiT2* mRNA expression in OMT1/DiT2 double cross lines, RT-PCR analysis was performed in 8-week-old plants. Leaf RNA was extracted using TRIzol reagent (Invitrogen, USA) and treated with DNase (Promega, USA). Using 1 µg of RNA, cDNA was synthesized by a first-stand cDNA synthesis kit (Roche Diagnostics, Switzerland), normalized to 100 ng µl$^{-1}$, and used for PCR analysis in a 10 µl reaction with gene-specific primers (see Supplementary Table S1). OseEF-1a was used as a positive and quality control. The PCR conditions were: pre-denaturation for 3 min, 95 °C; 40 cycles of the polymerization reaction consisting of a denaturation step for 20 s at 95 °C, for 30 s at 55 °C, and an extension step for 45 s 72 °C; and a final extension step for 3 min at 72 °C.

### Leaf chlorophyll content and plant growth analysis

The upper fully expanded leaves at mid-tillering stage (50–60 d old) were used to determine leaf chlorophyll content using a SPAD chlorophyll meter (Konica Minolta, Japan). The plant height and tiller number were measured at the booting stage from soil level to the base of the flag leaf on the main tiller.

### Western blot and immunodetection of recombinant protein (ZmOMT1)

The presence of the AcV5-tagged ZmOMT1 protein in leaf membrane extracts of *ZmOMT1* was checked by fractionating the isolated protein on a 12% SDS–PAGE gel, followed by western blot analysis. Primary mouse anti-AcV5 tag 1:2000 (Abcam plc, UK) and peroxidase-conjugated secondary [goat anti-mouse IgG (H+L) horseradish peroxidase (HRP), 1:2500, Thermo Fisher Scientific, Germany] antibodies were used for the detection of the AcV5 tag. The stained protein on nitrocellulose membranes was visualized by a LAS-4000 Mini luminescence image analyzer (GE Healthcare, Germany) using the ECL Western Blotting Detection Reagents (GE Healthcare, Germany).

### DNA blot analysis

Genomic DNA was extracted from the mature leaves using the potassium acetate method as described by Guillemaut and Maréchal-Drouard (1992). A total of 16 µg of genomic DNA was digested with *Hin*dIII restriction endonuclease (NEB Biolabs, USA), separated by electrophoresis on a 0.8% agarose gel, then transferred onto Hybond N+ membrane (GE Healthcare, UK). Blots were hybridized with a digoxigenin (DIG)-labeled *ZmPEPC* promoter-specific probe synthesized using the primers given in Supplementary Table S1 and the PCR DIG Probe Synthesis Kit (Roche Diagnostics, Switzerland). The signals were detected by CDP-Star (Roche Diagnostics, Switzerland) following the manufacturer's instructions.

### Immunolocalization

The seventh leaf at the mid-tillering stage was fixed and prepared for immunolocalization analysis as described in Lin *et al.* (2016). The fixed leaf sections were probed with the anti-AcV5 mouse monoclonal antibody (Abcam plc, UK) diluted 1:25 in blocking solution. Alexa Fluor 488 (fluorescent dye) goat anti-mouse IgG (Invitrogen, USA) secondary antibody was used for detection, and sections were examined on a BX61 using the Disk Scanning Unit attachment microscope (Olympus, Japan) with fluorescence functions.

### Total leaf membrane protein isolation

For protein extraction, the fully expanded third leaves at the mid-tillering stage were homogenized to a fine powder using a nitrogen-cooled mortar and pestle. Total leaf membrane protein was isolated from the powder using an extraction buffer consisting of 250 mM Tris (HCl, pH 8.5), 25 mM EDTA, 30% (w/v) sucrose, 5 mM DTT, and appropriate protease inhibitors. Two subsequent centrifugation steps at 10 000 *g* (10 min) and 100 000 *g* (45 min) were then performed, using a benchtop

centrifuge and ultracentrifuge, respectively. Ultimately, the isolated membrane was resuspended in 50 mM HEPES (KOH, pH 7.5), 5 mM EDTA, 2 mM DTT, together with protease inhibitors (Furbank *et al.*, 2001; Roell *et al.*, 2017). Finally, the protein concentration was measured utilizing the Pierce BCA Protein Assay Kit (Thermo Fisher Scientific, Germany) following the manufacturer's instructions.

### Reconstitution of total leaf membrane into liposomes

*In vitro* analysis of transporter activity was carried out using a freeze–thaw–sonication reconstitution procedure in concert with forward exchange of the substrate (Palmieri *et al.*, 1995). Following reconstitution, the proteoliposomes were pre-loaded with unlabeled malic acid to a final concentration of 30 mM (pH 7.5). Reconstituted proteins were separated from the non-reconstituted ones utilizing the size-based column chromatography technique [Sephadex G-25M columns (PD-10 column, GE Healthcare, USA)] (for the detailed procedure, see Roell *et al.*, 2017).

### [$^{14}$C]Malate uptake measurement

Uptake of radiolabeled substrates in counterexchange with non-labeled substrates was carried out at six different time points (2, 4, 8, 16, 32, and 64 min). The reaction was started by adding 950 µl of proteoliposomes into 50 µl of [$^{14}$C]malate diluted in transport medium (7 mM malic acid, pH 7.5), and stopped at each of the above-mentioned time points by loading 150 µl of the reaction mixture to an anion exchange resin column (acetate form, 100–200 mesh, Dowex AG1-X8 Resin, Bio-Rad, USA). The resin column was previously equilibrated five times using 150 mM sodium acetate (pH 7.5). Unincorporated [$^{14}$C]malate was replaced by acetate in the resin column and the incorporated label was washed through a scintillation vial containing 10 ml of Rotiszint® eco plus scintillation cocktail (Carl Roth, Germany). Finally, the uptake of radiolabeled substrate was measured as counts per minute (CPM) by scintillation counting. To correct for background and false positives, the entire experiment was repeated using proteoliposomes without pre-loading of the substrate of interest (for the detailed procedure, see Roell *et al.*, 2017). The uptake data were further assessed relative to both internal standards and total protein content (mg) in each sample. Related graphs were made using the one-phase association equation in GraphPad Prism 6 (http://www.graphpad.com/prism/prism.htm).

### Photosynthetic $CO_2$ assimilation, light response, and dark respiration rates

Leaf photosynthetic $CO_2$ assimilation and dark respiration rates during the tillering were measured on the middle portion of fully expanded leaves (two leaves per plant, three plants per line) in the standard leaf chamber of a portable photosynthesis system (LI-6400XT, LI-COR Biosciences, USA) between 08.00 h and 13.00 h at a constant airflow rate of 400 µmol s$^{-1}$, leaf temperature of 30 °C, and a leaf to air vapor pressure deficit of between 1.0 kPa and 1.5 kPa. Leaves were acclimated in the chamber for 30 min before measurements. The response curves of the net rate of $CO_2$ assimilation ($A$, µmol $CO_2$ m$^{-2}$ s$^{-1}$) to changing intercellular $CO_2$ concentration ($C_i$, µmol $CO_2$ mol$^{-1}$) were acquired by decreasing $C_a$ ($CO_2$ concentration in the cuvette) from 2000 µmol $CO_2$ mol$^{-1}$ to 20 µmol $CO_2$ mol$^{-1}$ at a photosynthetic photon flux density (PPFD) of 2000 µmol photons m$^{-2}$ s$^{-1}$. The 2 % oxygen entering the cuvette was set by mixing nitrogen and oxygen in the $CO_2$ free airstream through two mass flow controllers (model GFC17, Aalborg Mass Flow Systems, USA) at a flow rate of 1.5 ml min$^{-1}$. Maximum Rubisco activity ($V_{cmax}$) and maximum electron transport activity ($J_{max}$) were determined using the PsFit Model (Farquhar *et al.*, 1980; Bernacchi *et al.*, 2001, 2003). The light–response curves were measured by increasing the PPFD from 20 µmol photons m$^{-2}$ s$^{-1}$ to 2000 µmol photons m$^{-2}$ s$^{-1}$ at a $C_a$ of 400 µmol $CO_2$ mol$^{-1}$. The carboxylation efficiency (CE; µmol $CO_2$ m$^{-2}$ s$^{-1}$ µmol $CO_2$ mol$^{-1}$), $CO_2$ compensation point ($\Gamma$, µmol $CO_2$ m$^{-2}$ s$^{-1}$), and quantum yield ($\phi$, mol $CO_2$ mol$^{-1}$ photons) were calculated as described by Lin *et al.* (2016). The dark respiration rate ($R_d$, µmol $CO_2$ m$^{-2}$ s$^{-1}$) was measured on leaves in darkness following an acclimation at a PPFD of 1000 µmol photons m$^{-2}$ s$^{-1}$ for 10 min at a $C_a$ of 400 µmol $CO_2$ mol$^{-1}$, and calculated for 1100–1200 s in the dark.

### Leaf gas exchange and photosynthetic measurement in tandem with the metabolite analysis

To normalize metabolite pool sizes by photosynthetic flux, two sets of rice plants of different ages (set one, 30–35 d old; and set two, 50–55 d old) were analyzed. To measure $A$ and collect the samples for metabolite analysis under steady-state conditions, a custom gas exchange chamber was interfaced with a LI-COR 6400XT portable photosynthesis system (Supplementary Fig. S1B) encasing the leaf to be measured within a low gas-permeable sausage casing (5 cm diameter Nalophan, Kalle GmbH, Germany) to allow for rapid freeze-quenching of the sample. The chamber was constructed using two stainless-steel pipe sections fitted with Swagelok connections to the LI-COR sample line, one of which was capped on the end with a welded end cap. Prior to each measurement, an ~20 cm section of sausage casing was positioned between the pipe sections and sealed to the outside of the pipe sections using a small amount of silicone vacuum grease. The proximal end of a leaf blade was then sandwiched between two halves of a silicone stopper and inserted into the open pipe section with the adaxial side up. Actinic light was delivered via an LED ring light (Model R300, F&N Lighting, USA) which allowed constant, homogenous illumination of the leaf surface. Metabolic activity was rapidly quenched by freeze clamping the leaves with a liquid nitrogen-cooled copper disk attached to an aluminum handle. Fully expanded leaves of different tillers from five biological replicates were measured in the LICOR 6400XT that was attached to the sausage chamber. Flow through in the custom chamber was maintained at 700 µmol s$^{-1}$, light intensity at 500 µmol photons m$^{-2}$ s$^{-1}$, and $CO_2$ concentration was set to 200, 400, or 1000 µmol $CO_2$ mol$^{-1}$. Leaf surface area was determined by taking a photograph and analyzing in ImageJ v1.51m9 (Schneider *et al.*, 2012). Leaf temperature was not controlled but ranged between 25 °C and 27 °C as determined from energy balance calculations. Leaves were sealed within the chamber until steady-state net $CO_2$ fixation rates were reached and gas exchange measurements were logged. Next, the liquid nitrogen-cooled piston was inserted rapidly through the ring light onto the leaf and onto a plastic anvil, and then transferred rapidly to an aluminum foil pouch and into liquid nitrogen. To avoid potential diurnal artifacts, all measurements (genotypes and $CO_2$ treatments) were randomized and performed only during the peak photosynthetic activity of the rice plants between 09.00 h and to 15.00 h.

### Metabolite analysis (GC/MS)

The GC/MS-based metabolite measurements were performed as described by Fiehn (2007), using ribitol as an internal standard. Leaf samples were collected by rapid freeze-quenching from the custom gas exchange chamber describe above. Freeze-quenched tissue was ground into a fine powder in liquid nitrogen using a mortar and pestle. Extracted metabolites were injected into a gas chromatograph (Agilent 7890B GC System, Agilent Technologies, USA) that was in line with a mass spectrometer (Agilent 7200 Accurate-Mass Q-TOF GC/MS, Agilent Technologies, USA). Metabolite peaks were evaluated using Mass Hunter Software (Agilent Technologies, UAS). The relative amount of each metabolite was calculated from the peak area, considering both the initial fresh weight used for extraction and the internal standard.

*Total free amino acid (FAA) content*

FAA contents were measured using the ninhydrin colorimetric method as described by Smith and Agiza (1951), with minor changes. Briefly, FAA contents of 10 µl of metabolite extract were measured using the ninhydrin colorimetric method as described by Smith and Agiza (1951), with minor changes. A 10 µl aliquot of metabolite extract together with 40 µl of a methanol:water mixture (2.5:1 ratio) were added to 50 µl of 1 M citrate (NaOH, pH 5.2) and 100 µl of 1% (w/v) ninhydrin (prepared in methanol:$H_2O$, 2.5:1 ratio), and then heated to 95 °C for 20 min. The solution was then transferred to a microwell plate after a short centrifugation of 10 s at 10 000 rpm. The total amino acid content was then measured in a Synergy HT plate reader (BioTek, Germany) at a wavelength of 550 nm. Data were adjusted based on the L-leucine standard curve and related dilution factor.

*Starch and sucrose contents*

The youngest fully expanded leaf during the tillering stage was harvested at 10.00 h, frozen immediately, and ground in liquid nitrogen using a mortar and pestle. A 50 mg aliquot of homogenized leaf powder was then extracted in 500 µl of ice-cold 0.7 M perchloric acid and centrifuged at 21 100 *g* for 10 min at 4 °C to separate the soluble and insoluble fractions. The insoluble fraction containing the starch was further washed five times with 1 ml of 80% (v/v) ethanol. After centrifugation, the supernatant was discarded, the pellet was air-dried and resuspended in 500 µl of water, then gelatinized by boiling for 4 h and hydrolyzed overnight at 37 °C with 0.5 U of amyloglucosidase and 5 U of α-amylase. The starch content was measured as described in Smith and Zeeman (2006). The soluble fraction containing sucrose was neutralized to pH 6 with neutralization buffer (2 M KOH, 0.4 M MES, 0.4 M KCl). After centrifugation at 21 100 *g* for 10 min at 4 °C, the supernatant was assayed for sucrose content by enzymatic determination as described by Smith and Zeeman (2006).

*Carbon:nitrogen (C:N) ratio measurement*

The ratio of carbon to nitrogen as well as $\delta^{13}C$ were analyzed based on leaf dry weight (mg) of 30-day-old and 50-day-old transgenic plants using the ISOTOPE cube elemental analyzer connected to an Isoprime 100 isotope ratio mass spectrometer (Elementar, Germany). The $\delta^{13}C$ ratio is expressed as parts per thousand (‰) using the international standard of the Vienna Pee Dee Belemnite (VPDB).

*Transmission electron microscopy*

Rice seeds were germinated in Petri dishes in distilled water for 4 d and then placed on a floating net in distilled water in a 19 liter bin in greenhouses at the University of Toronto. Seedlings were fertilized with 1/3 strength hydroponic media at day three after transfer and then with full-strength media every 4 d (Makino and Osmond, 1991). Plants were sampled from 09.30 h to 11.00 h when day length was >11.5 h and light intensity in the unshaded greenhouse regularly exceeded 1400 µmol photons $m^{-2}$ $s^{-1}$. The middle section of the most recently fully expanded leaf was dissected into 2 mm pieces, prepared in Araldite 502 epoxy resin, and sectioned for TEM as described by Khoshravesh *et al.* (2017). Sections were imaged with a Phillips 201 transmission electron microscope equipped with an Advantage HR camera system (Advanced Microscopy Techniques, USA).

*Generation of rice lines overexpressing both ZmOMT1 and ZmDiT2*

To generate transgenic rice plants co-expressing *ZmOMT1* and *ZmDiT2*, homozygous *ZmOMT1* single transgenic $T_2$ lines (OMT1-79, OMT1-80, and OMT1-45) were crossed with homozygous *ZmDiT2* single

transgenic $T_2$ lines (DiT2-27, DiT2-39, and DiT2-44) (Supplementary Fig. S2A). The $F_1$ progeny were selfed to produce segregating $F_2$ populations. The pSC110:*ZmDiT2*:AcV5 construct used for generating DiT2 lines contained the coding sequence of *ZmDiT2* (GRMZM2G40933) from *Zea mays* of the B73 variety and included an AcV5 epitope tag at the C-terminal end of the coding sequence. *ZmDiT2* was cloned using the primers shown in Supplementary Table S1. Homozygous *ZmDiT2* lines were selected by PCR analysis, and protein accumulation was determined on western blots (Supplementary Fig. S2B).

# Results

## *Three independent single transgene insertion lines accumulate ZmOMT1 protein in mesophyll cells*

A total of 198 $T_0$ plants were generated, of which 87 were positive for *ZmOMT1* as determined by PCR analysis of genomic DNA, and 40 of which carried a single copy of the *ZmOMT1* transgene as determined by DNA gel blot analysis. Three single insertion lines (OMT1-79, OMT1-80, and OMT1-87; Supplementary Fig. S3) were advanced to succeeding generations to obtain homozygous lines. Homozygous plants in either the $T_3$ or $T_4$ generation were used for all subsequent experiments. To compare steady-state transcript levels of native rice *OsOMT1* and the introduced *ZmOMT1*, qRT-PCR was performed. Expression of the native *OsOMT1* was not affected by expression of *ZmOMT1* in any of the three overexpressing lines, with transcript levels observed similar to those in wild-type rice (Fig. 1A ). *ZmOMT1* transcripts accumulated in all three lines, with the highest levels in OMT1-79 and the lowest in OMT1-80 (Fig. 1A). To test whether the high amounts of *ZmOMT1* mRNA in the transgenic lines were accompanied by increased transporter protein abundance, the amounts of ZmOMT1 protein in extracted total membrane leaf protein were examined via western blot, taking advantage of the C-terminal AcV5 tag. The ZmOMT1 protein was clearly detectable in all three lines (OMT1-79, OMT1-80, and OMT1-87) by immunoblotting (Fig. 1B). As with the transcript levels, OMT1-79 and OMT1-87 lines accumulated more ZmOMT1 protein than the OMT1-80 line. We further examined the spatial localization of ZmOMT1 in the transgenic lines by immunolocalization. Figure 1C shows that the ZmOMT1 protein accumulated primarily in chloroplasts of mesophyll cells. Collectively, these data show that the *ZmPEPC* promoter drives expression of *ZmOMT1* predominantly in mesophyll cells of rice leaf tissues and that the protein can be detected in the chloroplasts of those cells.

## *OMT1 membrane transporter activity is significantly increased in transgenic rice lines*

To test whether expression of the *ZmOMT1* transgene led to increased OMT1 transporter activity in transgenic lines, we measured malate counterexchange activity in liposomes reconstituted with membrane proteins isolated from the wild type and overexpressing lines (Fig. 2A). We detected significantly

higher malate–malate counterexchange activity in liposomes reconstituted with membrane proteins from overexpression lines as compared with those reconstituted with membrane proteins isolated from the wild type. These data clearly indicate that the recombinantly introduced ZmOMT1 transporter protein is active in rice (Fig. 2B).

### Slower growth and leaf lesion phenotypes of OMT1 lines

The transgenic plants with the highest ZmOMT1 protein levels (OMT1-79 and OMT1-87) displayed perturbed phenotypes at the whole-plant level. The OMT1-79 and OMT1-87 lines were shorter (Fig. 3A; Table 1) than the wild type and displayed lesions in mature leaves in IRRI (Fig. 3B). An ELISA test for detection of infection caused by tungro virus was negative (data not shown), indicating that the lesions were not caused by tungro virus infection. The OMT1-80 line that accumulates lower levels of ZmOMT1 (Fig. 1) had more and

longer tillers compared with the wild type (Fig. 3A; Table 1) and did not have a lesion–mimic phenotype (Fig. 3B). Despite the different lesion–mimic phenotypes, chlorophyll content was similar in the youngest fully expanded leaves of all three transgenic lines and the wild type (Table 1). These results suggest that high levels of *ZmOMT1* expression in rice inhibit plant growth and induce a lesion–mimic phenotype in mature leaves, without altering chlorophyll content in young leaves. The symptom is due to the accumulation of the substrates transported by OMT1 and shows the clear phenotypes in more mature leaves.

### Photorespiratory-deficient phenotypes of ZmOMT1 transgenic lines

To examine the effect of overexpressing ZmOMT1 on photosynthesis in response to changing light conditions, the $CO_2$ assimilation rate (*A*) in response to PPFD was measured at ambient $CO_2$ conditions (400 μmol $CO_2$ $mol^{-1}$). The transgenic lines
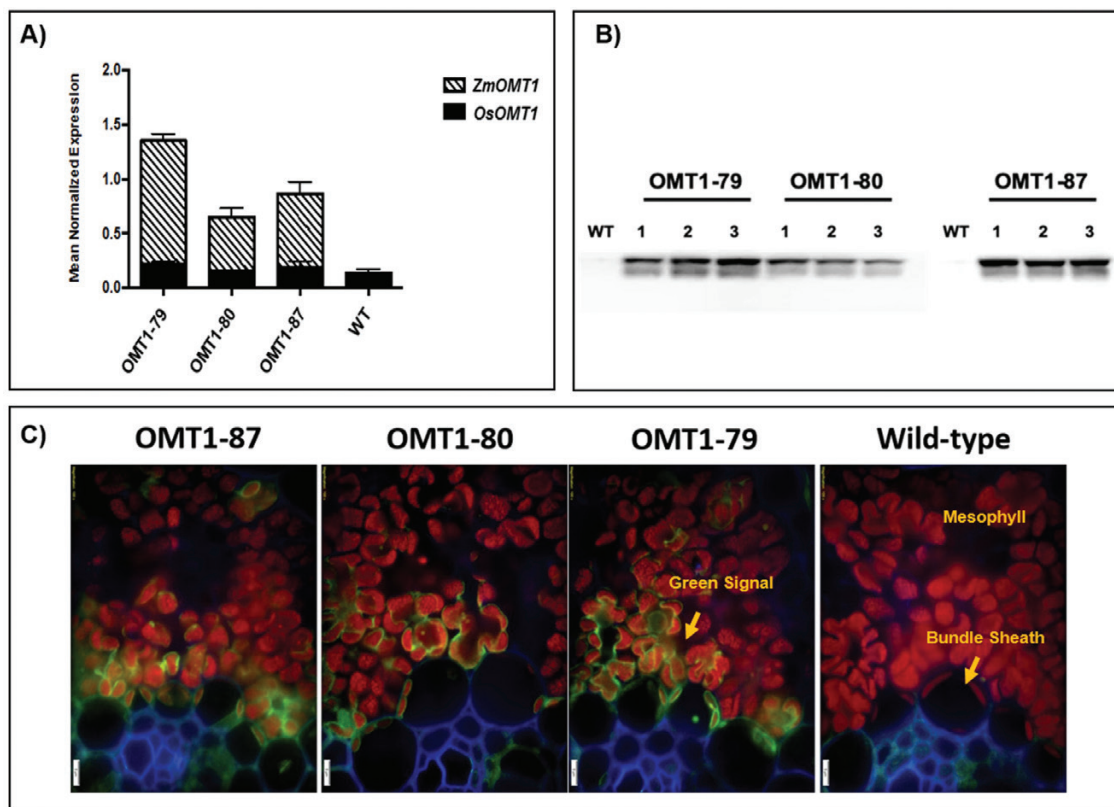


**Fig. 1.** Transcript accumulation of *OsOMT1* and *ZmOMT1* genes detected by qRT-PCR analysis on leaf blades of transgenic rice OMT1 lines (OMT1-79, OMT1-80, and OMT1-87). Wild-type plants (WT) served as a control. Data represent the mean normalized expression ±SEM of three and two biological and technical replicates, respectively (A). Assessment of expressed ZmOMT1 protein in transgenic lines (OMT1-79, OMT1-80, and OMT1-87) together with WT rice as a control via western blot using 12% SDS–PAGE and two-step antibody immunodetection with 5 s exposure time. The calculated molecular mass of OMT1-AcV5 is ~60 kDa; however, 40 kDa is the size shown on the blot. Samples were loaded based on equal leaf area of 0.396 $cm^2$ (B). Immunolocalization of *Zm*OMT1-AcV5 protein in leaves of WT, OMT1-79, OMT1-80, and OMT1-87 plants in which the green signal is easiest to see in line OMT1-79 where the levels are highest. Anti-AcV5 tag primary antibody diluted 1:25 plus Alexa Fluor 488 (fluorescent dye) goat anti-mouse IgG secondary antibody diluted 1:200 was used to probe for the AcV5 tag (shown in green color). Chlorophylls are shown as a red autofluorescence. The cell wall was co-stained with calcofluor white and is shown in blue. Magnification: ×200. Scale bar: 5 μm (C).
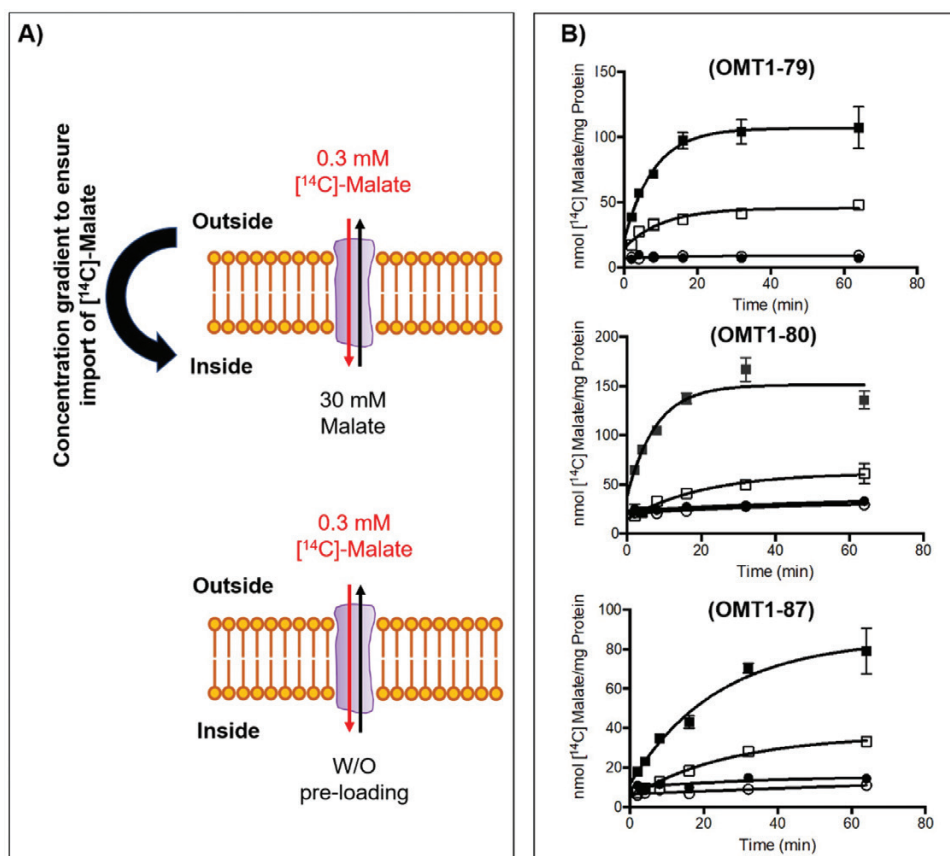
**Fig. 2.** Illustration of proteoliposome uptake assay after reconstitution of total leaf membrane protein from transgenic lines and wild-type controls. Uptake of [$^{14}$C]malate (from outside into the inside of liposome) was measured with 30 mM or without (w/o) pre-loading of unlabeled malate inside the proteoliposome. Transport was initiated by adding [$^{14}$C]malate to a final concentration of 0.3 mM (A). Uptake of malate into liposomes reconstituted with total crude membrane protein isolated from three different transgenic OMT1 lines, overexpressing *ZmOMT1* (OMT1-79, OMT1-80, and OMT1-87), preloaded with either 30 mM malate (closed squares) or without preloading (closed circles) respectively. Liposomes reconstituted with total crude membrane protein isolated from WT plants, preloaded with either 30 mM malate (open squares) or without preloading (open circles) respectively served as controls. Values represent the arithmetic means ± SEM, *n* = 3 (B).

with highest *ZmOMT1* expression (OMT1-79 and OMT1-87) had slightly lower $CO_2$ assimilation rates than the wild type, whereas OMT1-80 had a similar rate (Fig. 4A). At 2000 μmol photon m$^{-2}$ s$^{-1}$, photosynthesis in the OMT-80 line and wild type was already saturated, but this was not the case for OMT-79 and OMT-87 lines. The *ZmOMT1*-overexpressing lines had similar quantum efficiency (QE) from the initial slope of light response curves (PPFD <100 μmol photons m$^{-2}$ s$^{-1}$) to the wild type (Table 2), suggesting that overexpressing ZmOMT1 protein does not affect the efficiency of using light energy to fix $CO_2$ in rice plants. The dark respiration rates were twice as high in OMT1-79 and OMT1-87 lines compared with OMT1-80 and the wild type (Table 2), suggesting that the carbon balance is possibly altered in OMT1-79 and OMT1-87 compared with the wild type. Moreover, the $CO_2$ assimilation rate (*A*) in response to intercellular $CO_2$ concentration (*C*$_i$) under non–photorespiratory (2% $O_2$) versus photorespiratory (21% $O_2$) conditions was measured under saturating light intensity of 2000 μmol photons m$^{-2}$ s$^{-1}$. At 21% $O_2$, lower photosynthetic rates were observed in

OMT1-79 and OMT1-87 lines compared with the wild type and the OMT1-80 line (Fig. 4B). OMT1-79 and OMT1-87 lines also had lower CEs and OMT1-79 had higher $CO_2$ compensation points (Γ) (Table 2). Under low photorespiratory conditions (2% $O_2$), the wild type, OMT1-80, and OMT1-87 had similar photosynthetic rates at ~40 μmol $CO_2$ m$^2$ s$^{-1}$, and similar Γ (Fig. 4C). Above a *C*$_i$ of 400 μmol $CO_2$ mol$^{-1}$, the assimilation rate was lower in OMT1-79 and OMT1-87 lines. The maximum rate of Rubisco carboxylation ($V_{cmax}$) and the maximum rate of electron transport ($J_{max}$) were reduced in OMT1-79 and OMT1-87 lines under high photorespiratory conditions (Supplementary Table S2). Together, these results indicate that the transgenic lines are Rubisco limited under high photorespiratory conditions (21% $O_2$) and that when *ZmOMT1* is expressed, ribulose 1,5-bisphosphate (RuBP) regeneration is limited at high $CO_2$ concentrations. Together, these data indicate that *ZmOMT1* overexpression leads to higher rates of photorespiration, a suggestion supported by the observation that transgenic lines have a higher Γ than the wild type at 21% but not at 2% $O_2$.
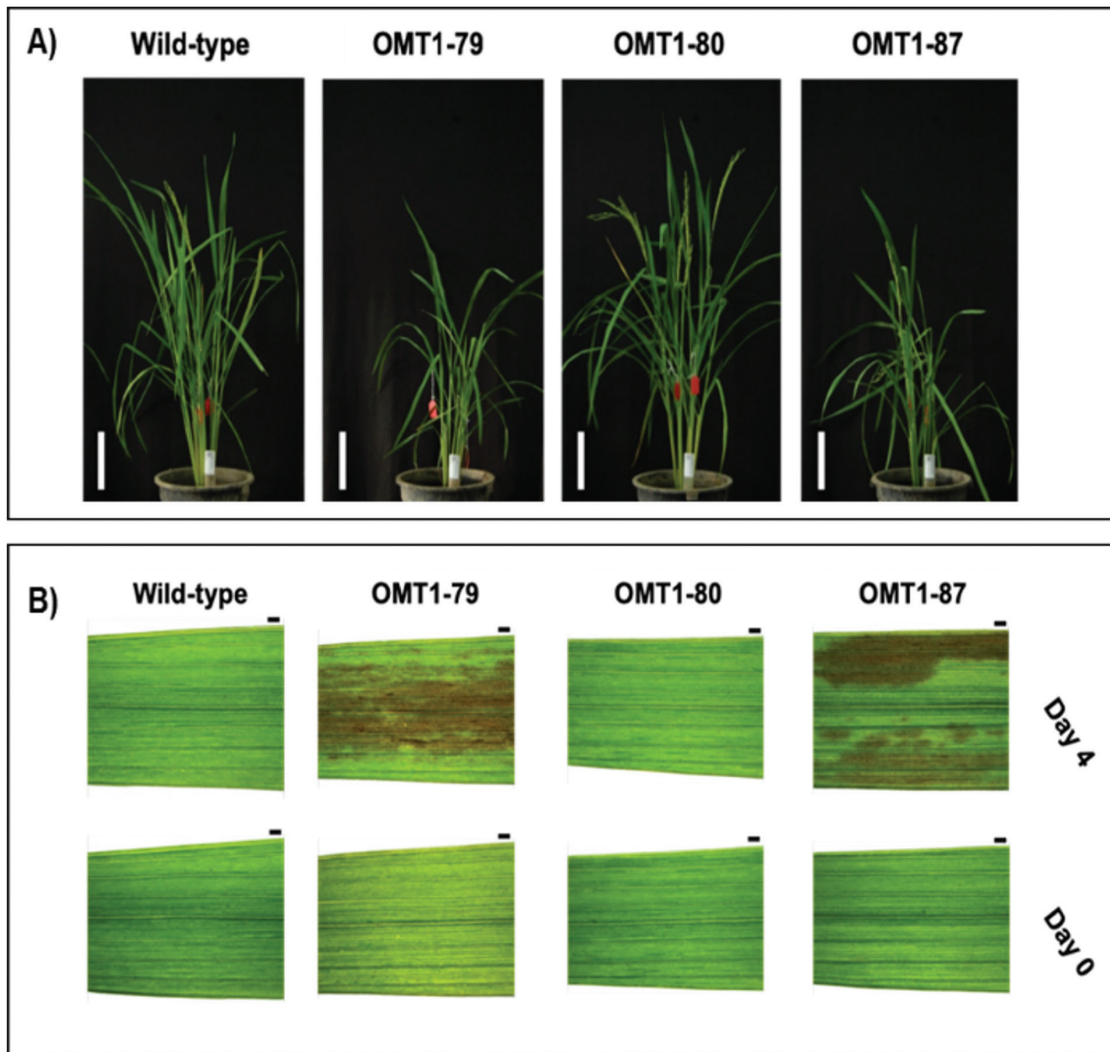
**Fig. 3.** Representative pictures of wild-type, OMT1-79, OMT1-80, and OMT1-87 lines grown under ambient conditions; 70 d post-germination. Scale bar: 15 cm (A). Representative pictures of the youngest fully expanded leaves (Day 0) and the same leaves after 4 d (Day 4) of wild-type, OMT1-79, OMT1-80, and OMT1-87 plants. The middle portions of the youngest fully expanded leaves were taken when their next leaf needles started to emerge (Day 0) and the same positions from the same leaves were taken after 4 d (Day 4). Scale bar: 1 mm (B).

**Table 1.** Leaf chlorophyll content, plant height, and tiller number of wild-type and OMT1 lines

|  | Chl (SPAD value) | Tiller number | Plant height (cm) |
|---|---|---|---|
| **Wild type** | 42.1 ± 0.7ns | 9 ± 0.5 ab | 56.4 ± 1.1 a |
| **OMT1-79** | 42.4 ± 1.4ns | 8 ± 2 b | 42.3 ± 0.4 c |
| **OMT1-80** | 41.3 ± 1ns | 12 ± 1 a | 60 ± 1.5 a |
| **OMT1-87** | 42.2 ± 0.8ns | 6.8 ± 0.9 b | 47.8 ± 2.9 b |

Chlorophyll SPAD values are the average ±SEM of three leaves from four plants at mid-tillering stage using the upper fully expanded leaves. Tiller number and plant height are the average ±SEM of four individual $T_3$ plants; 70 d post-germination. Different letters within groups indicate that values are statistically different $P \leq 0.05$, Tukey's multiple comparison test. ns indicates non-significant, $P > 0.05$.

### Chloroplast ultrastructure is perturbed in OMT1 transgenic lines

The macroscopic and physiological phenotypes of OMT1 lines were accompanied by ultrastructural changes in mesophyll cell chloroplasts. In contrast to wild-type plants, mesophyll cell chloroplasts of the OMT1 lines developed a peripheral reticulum (PR; Fig. 5) which is an internal network of tubules and vesicles continuous with the chloroplast inner envelope (Rosado-Alberio *et al.*, 1968; Laetsch, 1974). Plastoglobules (PGs), not observed in wild-type plants, were also present in chloroplasts of the overexpressing lines. PGs are lipid microcompartments posited to function in lipid metabolism, redox and photosynthetic regulation, and thylakoid repair and disposal during chloroplast biogenesis and stress (Rottet *et al.*, 2015; van Wijk and Kessler, 2017).

### $CO_2$ assimilation rate and leaf metabolite profiles of transgenic lines

The photosynthetic rate of the older ZmOMT1 transgenic plants (50–55 d old) measured in our custom-built gas exchange cuvette (Supplementary Fig. S1B) was affected more
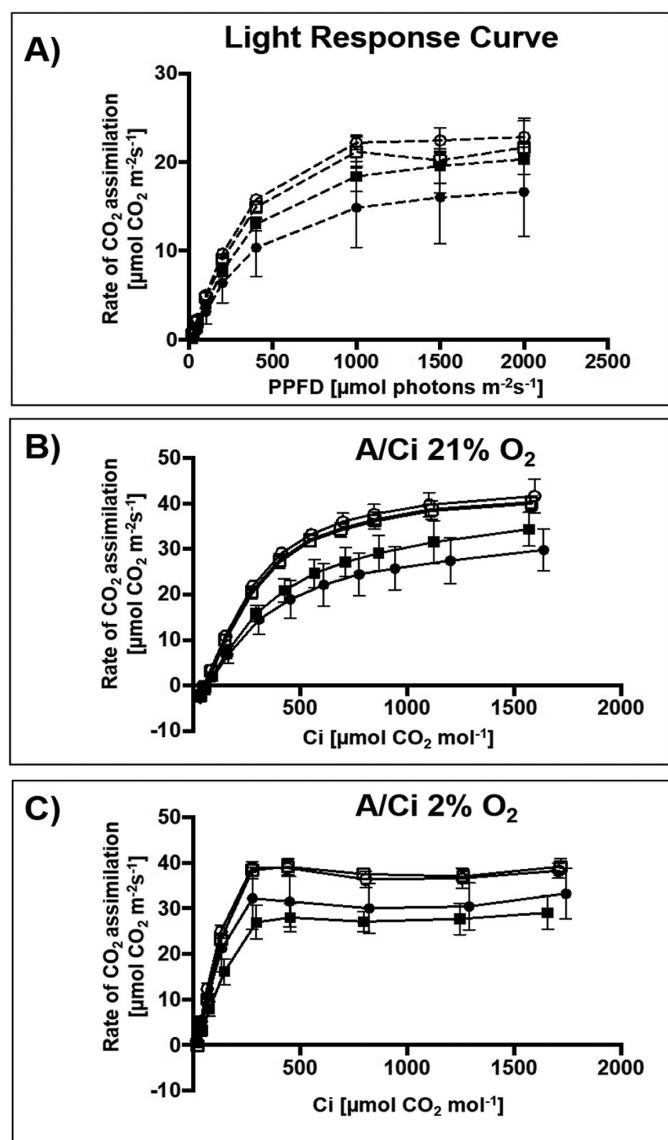
**Fig. 4.** Rate of $CO_2$ assimilation (*A*) in response to photosynthetic photon flux density (PPFD). Light–response curve measurements were carried out under 400 µmol $CO_2$ mol$^{-1}$ and leaf temperature of 30 °C. Values represent the mean ±SEM of two leaves of four individual T$_4$ plants of OMT1 lines (OMT1-79, OMT1-80, and OMT1-87) and wild-type rice (WT) (A). Rate of $CO_2$ assimilation in response to intercellular $CO_2$ concentration ($C_i$) at 21% (B) and 2% $O_2$ (C). The measurements were carried out under a light intensity of 2000 µmol photons m$^{-2}$ s$^{-1}$ at a leaf temperature of 30 °C. Values represent the mean ±SEM of two leaves of four individual T$_4$ plants of OMT1 lines (OMT1-79, black square; OMT1-80, white square; and OMT1-87, black circle) and WT rice, white circle.

than that of younger plants (30–35 d old) (Fig. 6A and B). In younger plants, there was no significant difference in photosynthetic rate between the wild type and any of the *ZmOMT1* transgenic plants. However, in older plants, the photosynthetic rate was significantly lower in *ZmOMT1* transgenic lines under ambient $CO_2$ concentration (400 ppm) in each of the transgenic lines (Fig. 6B). The photosynthetic rate was partially restored under high $CO_2$ concentration (1000 ppm) for older

plants and only one line had a significantly lower photosynthetic rate as compared with the wild type under 200 ppm $CO_2$ (Fig. 6B).

### Metabolite profiles of ZmOMT1 lines and wild-type rice reveal altered steady-state pools of TCA intermediates and aspartate

The metabolic state of 30- to 35-day-old *ZmOMT1* transgenic rice lines and the wild type under different $CO_2$ conditions was examined using GC-MS analysis. Large differences were observed among the measured metabolites of the mitochondrial tricarboxylic acid (TCA) cycle between the transgenic lines and the wild type. Malic acid, fumaric acid, iso-citric acid, succinic acid, and 2-oxoglutarate were significantly lower in all *ZmOMT1* transgenic rice lines than in the wild type under different $CO_2$ concentrations (Fig. 7A). Among photorespiratory intermediates, only glyceric acid displayed a lower amount in OMT1 lines. Others, such as glycolic acid, glycine, and serine, were similar to the wild type or tended to be higher, in some cases significantly (Fig. 7B). Of the substrates transported by OMT1 and DiT2, aspartic acid was significantly increased in the overexpression lines (Fig. 7C). Malic acid and 2-oxoglutarate, as previously mentioned, were significantly lower and glutamic acid remained unchanged for all three OMT1 transgenic rice lines in comparison with the wild type under different $CO_2$ concentrations (Fig. 7A, C). We further calculated the aspartate/malate ratio for all transgenic rice lines and compared them with the wild type. As shown in Fig. 7D, the aspartate to malate ratio was significantly higher in transgenic *ZmOMT1* lines relative to the wild type under different $CO_2$ concentrations.

### Total free amino acids, carbon:nitrogen ratios, and carbohydrate contents are decreased in leaves of ZmOMT1 lines

The absolute FAA contents of *ZmOMT1* lines and wild-type rice were determined to assess the effect of altered plastidial dicarboxylate transport capacity on amino acid metabolism. Amounts were lower in older plants of *ZmOMT1* lines (50–55 d old) under all $CO_2$ concentrations but were significantly decreased under ambient $CO_2$ (400 ppm) compared with wild-type rice (Fig. 8A). As plants aged, the C:N ratio also decreased significantly in *ZmOMT1* transgenic lines, but the $\delta^{13}C$ value did not differ between the wild type and transgenic lines (Fig. 8B). Sucrose and starch amounts were significantly reduced in the OMT1 lines compared with wild-type plants (Fig. 8C).

### Simultaneous expression of ZmOMT1 and ZmDiT2 in transgenic rice lines restored the wild-type growth phenotype

We hypothesized that the phenotypes observed in rice lines overexpressing *ZmOMT1* might be caused by an

**Table 2.** Comparison of photosynthesis parameters.

| | QE (µmol $CO_2$ m$^{-2}$ s$^{-1}$ µmol photons mol$^{-1}$) | $R_d$ (µmol $CO_2$ m$^{-2}$ s$^{-1}$) | Γ (µmol $CO_2$ m$^{-2}$ s$^{-1}$) | CE (µmol $CO_2$ m$^{-2}$ s$^{-1}$ µmol $CO_2$ mol$^{-1}$) | Γ (µmol $CO_2$ m$^{-2}$ s$^{-1}$) | CE (µmol $CO_2$ m$^{-2}$ s$^{-1}$ µmol $CO_2$ mol$^{-1}$) |
|---|---|---|---|---|---|---|
| | | | 21% $O_2$ | | 2% $O_2$ | |
| **Wild type** | 0.05 ± 0.003ns | 0.42 ± 0.26 a | 54.86 ± 5.23 b | 0.12 ± 0.01 a | 13.72 ± 1.93 ns | 0.23 ± 0.013 a |
| **OMT1-79** | 0.043 ± 0.003ns | 0.93 ± 0.20 ab | 64.55 ± 3.47 b | 0.08 ± 0.01 bc | 17.89 ± 4.76 ns | 0.12 ± 0.02 b |
| **OMT1-80** | 0.047 ± 0.002ns | 0.41 ± 0.21 a | 53.81 ± 3.17 b | 0.11 ± 0.01 ab | 22.63 ± 0.8 ns | 0.22 ± 0.2 a |
| **OMT1-87** | 0.037 ± 0.011ns | 1.06 ± 0.12 b | 67.9 ± 7.23 a | 0.07 ± 0.02 c | 12.55 ± 6.54 ns | 0.17 ± 0.05 ab |

Measurements of quantum efficiency (QE) were made at 400 µmol $CO_2$ mol$^{-1}$ and a leaf temperature of 30 °C. Values represent the mean ±SEM of two leaves from four individual $T_4$ generation plants. Measurements of dark respiration rate ($R_d$) were made on leaves dark adapted for 1100 s. Values represent the mean ±SEM of measurements made every 10 s for 100 s from two leaves of four individual $T_4$ generation plants. Measurements of $CO_2$ compensation point (Γ) and carboxylation efficiency (CE) were made at a photosynthetic photon flux density (PPFD) of 2000 µmol photons m$^{-2}$ s$^{-1}$ and a leaf temperature of 30 °C at either 21% or 2% $O_2$. Values represent the mean ±SEM of two leaves of four individual $T_4$ generation plants. Different letters within groups indicate that values are statistically different $P \leq 0.05$, Tukey's multiple comparison test. ns indicates non-significant, $P > 0.05$.
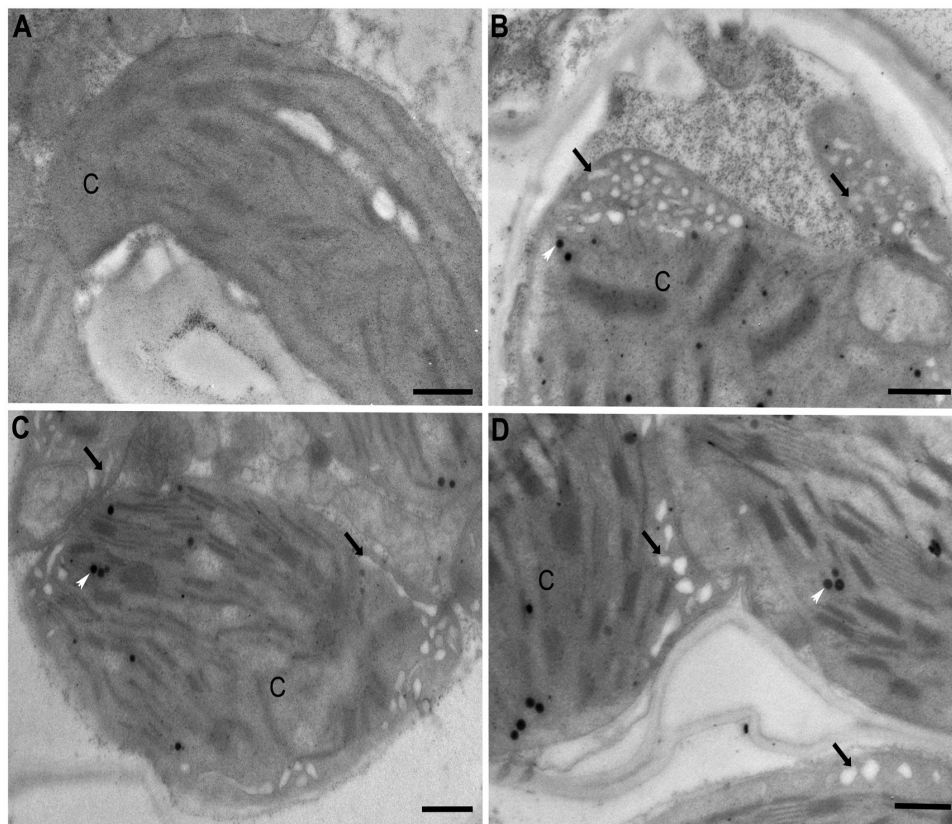


**Fig. 5.** Transmission electron micrographs illustrating chloroplasts without peripheral reticulum in the wild type (A) and with peripheral reticulum (black arrows) in OMT1 transgenic lines OMT1-79 (B), OMT1-80 (C), and OMT1-87 (D). White arrows mark plastoglobules; C, chloroplast; Scale bar=500 nm.

imbalance between the transport capacities for malate, OAA, and 2-oxoglutarate (transported by OMT1), and glutamate and aspartate (transported by DiT2). If this assumption was true, then the phenotypes of *ZmOMT1* single transgenic lines should be rescued by simultaneous overexpression of *ZmDiT2*. We hence generated double transgenic lines in which both *ZmOMT1* and *ZmDiT2* were expressed (Supplementary Figs S5, S6). Notably, double transgenic lines displayed similar physiological phenotypes as wild–type plants when grown under ambient conditions (Fig. 9). Leaf chlorophyll content, number of tillers, and plant height were comparable with those of the wild type in two of three independent *ZmOMT1/ ZmDiT2* double overexpressing plants.

## Discussion

$C_4$ plants require a higher transport capacity for OAA and malate across the chloroplast envelope of leaf mesophyll cells
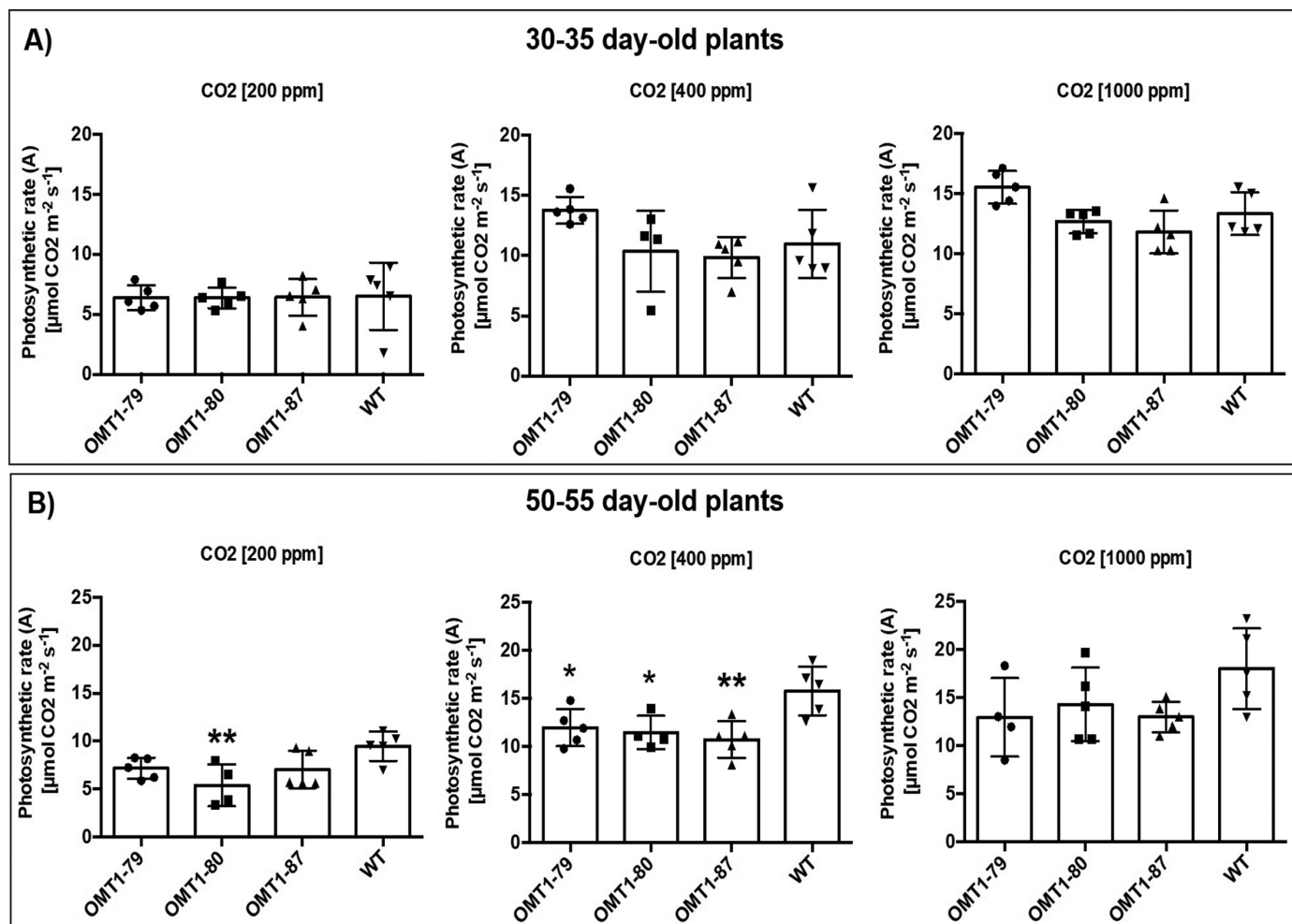
**Fig. 6.** Impact of three $CO_2$ concentrations (200, 400, and 1000 $\mu$mol $CO_2$ mol$^{-1}$) on the rate of $CO_2$ assimilation (*A*) measured inside a custom gas exchange cuvette of two different plants sets [OMT1 lines (OMT1-79, OMT1-80, and OMT1-87) and the wild type (WT)]; younger, 30–35 d old (A) and older, 50–55 d old (B). For both experiments, the youngest, fully expanded leaf was chosen for each treatment. Values represent the mean ±SEM, *n*=4–5. Significant differences from the WT are indicated by *$P\leq$0.05 and **$P\leq$0.01, Tukey's multiple comparison test.

because OAA generated by the PEPC reaction in the cyto-plasm is further converted to malate by plastidial NADP-MDH. Malate is then exported from mesophyll chloroplasts and transported to the carbon-concentrating sheath cells. In this study, as part of the effort to engineer $C_4$ rice, transgenic rice lines were generated that overexpress the gene encoding the chloroplast envelope OAA/malate/2-oxoglutarate antiporter OMT1 from maize, *ZmOMT1*.

A striking feature of chloroplasts in the *ZmOMT1*-overexpressing lines was the development of the PR. This peripheral matrix of tubules and vesicles is continuous with the inner envelope which is the site where metabolite exchange occurs (Pottosin and Shabala, 2016). Although PR has been reported to be present in mesophyll and bundle sheath cells of other $C_3$ grasses such as wheat (Szczepanik and Sowinski, 2014), this cellular feature has not been observed in other *Oryza* species or cultivars (Sage and Sage, 2009; Giuliani *et al.*, 2013). The PR is also present in mesophyll and sheath cells of

$C_4$ species of grasses and eudicots, although, in comparison with $C_3$ grasses, the PR in $C_4$ species is much more abundant (Laetsch, 1968, 1969; Rosado-Alberio *et al.*, 1968; Szczepanik and Sowinski, 2014). Chloroplast envelope proliferation in association with overexpression of envelope proteins has been previously reported (Breuers *et al.*, 2012), supporting the idea that the ZmOMT1 transporter is accumulating to high amounts in the inner envelope of mesophyll chloroplasts. Given that the presence of the PR is posited to be correlated with high rates of metabolite exchange (Hilliard and West, 1971; Gracen *et al.*, 1972*a, b*; Laetsch, 1974), the PR phenotype in *ZmOMT1* transgenic lines is consistent with the altered metabolic profiles observed.

In general, OAA transported by OMT1 enters the chloroplast and is subsequently converted either to malate by NADP-MDH or to aspartate by plastidial aspartate aminotransferase. Whereas malate can be transported back to the cytosol by OMT1, export of aspartate out of chloroplasts requires the
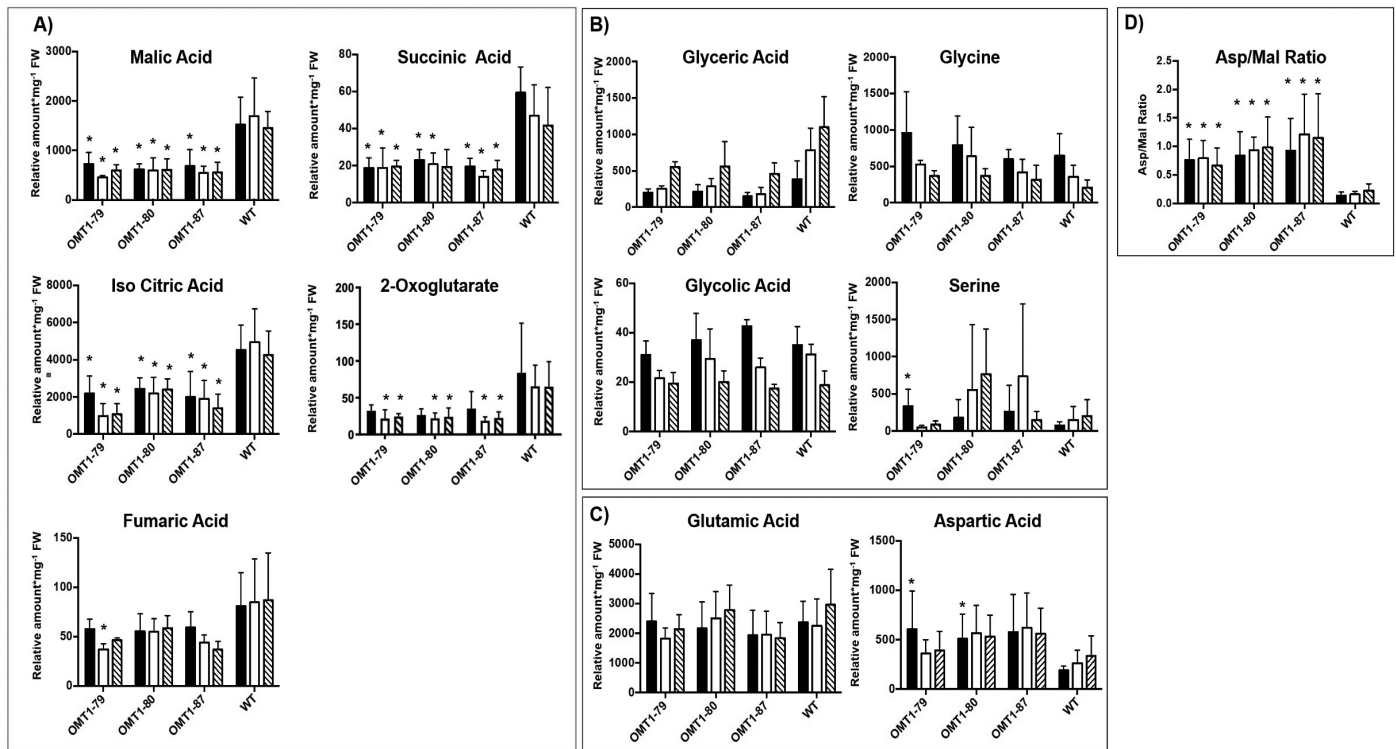
**Fig. 7.** Relative amount of metabolites involved in the citric acid cycle (A), in photorespiration (B), in the key substrates of OMT1 and DiT2 membrane transporters (C), and the aspartate/malate ratio (D) of OMT1 lines (OMT1-79, OMT1-80 and OMT1-87) and wild-type (WT) rice leaves under different $CO_2$ concentrations [µmol $CO_2$ mol$^{-1}$] (200, black; 400, white; and 1000, dashed pattern). Values represent the mean ±SEM, *n*=5; significant differences from the WT are indicated by *$P \leq 0.05$, Student's *t*-test.

activity of DiT2. Enhanced accumulation of aspartate in the transgenic lines (Fig. 7D) indicates that this metabolite cannot be further metabolized in chloroplasts and thus that metabolite flux between chloroplasts and mitochondria is blocked. This outcome could explain the lower amounts of intermediate metabolites in the TCA cycle of mitochondria (the energy machinery) (Fig. 7A) among which a few are common substrates of the OMT1 transporter (Fig. 7A, C). All these intermediates are pivotal for effective function of plant metabolic pathways. For instance, malate, a primary substrate of OMT1, participates as an intermediate in many vital mechanisms in the cytosol and vacuole (redox homeostasis, pH levels, and carbon storage) (Fernie and Martinoia, 2009). Loss-of-function mutations in *OMT1* in the C$_3$ plants Arabidopsis (Kinoshita *et al.*, 2011) and tobacco (Schneidereit *et al.*, 2006) caused an increase in levels of 2-oxoglutarate and malate and a decrease in levels of aspartate, the opposite trend to that seen in *ZmOMT1*-overexpressing rice plants. Surprisingly, any disruption to OMT1 activity (either an increase or a decrease) leads to lower photosynthetic rates than the wild type, suggesting that OMT1 transporter activity must be precisely regulated to maintain optimal photosynthetic performance. The reduced photosynthetic rates in *ZmOMT1* transgenic rice plants reveal possible relationships between photosynthesis, photorespiration, and cellular redox status. Differences in photosynthesis

were significant in the plants measured in the Philippines and in older plants grown in Düsseldorf, Germany (Figs 4A, 6B). This decrease in photosynthesis is only partially explained by increases in $R_d$ (Table 2). Interestingly, this decrease in photosynthesis could be rescued by minimizing photorespiration under some measurement and growth conditions, but not others. Specifically, the photosynthetic rates of *ZmOMT1* transgenic lines were not rescued by elevated $CO_2$ or reduced $O_2$ when measured under growth conditions in the Philippines (Fig. 4B, C), but were rescued in the plants grown in Düsseldorf, Germany when measured under elevated $CO_2$ (Fig. 6). One major difference in these measurements was the light intensity used (2000 µmol m$^{-2}$ s$^{-1}$ for the $A$–$C_i$ curves versus 500 µmol m$^{-2}$ s$^{-1}$ for the metabolite assays), meaning that phenotypic rescue may only occur under subsaturating light intensities. As photorespiratory rates increase, the increased demand for ATP relative to NAD(P)H pushes the redox status of the NADP$^+$/ NADPH pools to be more reduced unless processes either decrease plastidic NADPH (malate valve) or increase ATP production (cyclic electron flux around PSI). The oxidation of NADPH, which could be increased with increased export of malate, must be finely balanced with metabolic demand so as not to directly compete with NADPH pools needed to supply the Calvin–Benson cycle or photorespiration. Under subsaturating light, there are numerous lines of evidence

suggesting that the malate valve regulates this balance, particularly under photorespiratory conditions (Kramer and Evans, 2011; Walker *et al.*, 2014; Shameer *et al.*, 2019). In particular, this event leads to the reduced provision of carbon skeletons for nitrogen assimilation and to a significant reduction of the leaf C:N ratio (Fig. 8B) together with the reduction of FAA in the older OMT1 transgenic lines under 400 ppm $CO_2$ concentration (Fig. 8A). Principally, both carbohydrate and amino

acid biosynthesis are relying on each other (Nunes–Nesi *et al.*, 2010). Correspondingly, in all three OMT1 transgenic lines, both sucrose and starch contents were decreased significantly compared with wild–type rice (Fig. 8C). It is known that a part of the photoassimilated carbon during the day will be partitioned and stored as starch to be used later during the night as a source of energy supply for sink tissues as well as fatty acid and amino acid biogenesis (Stitt and Zeeman, 2012).
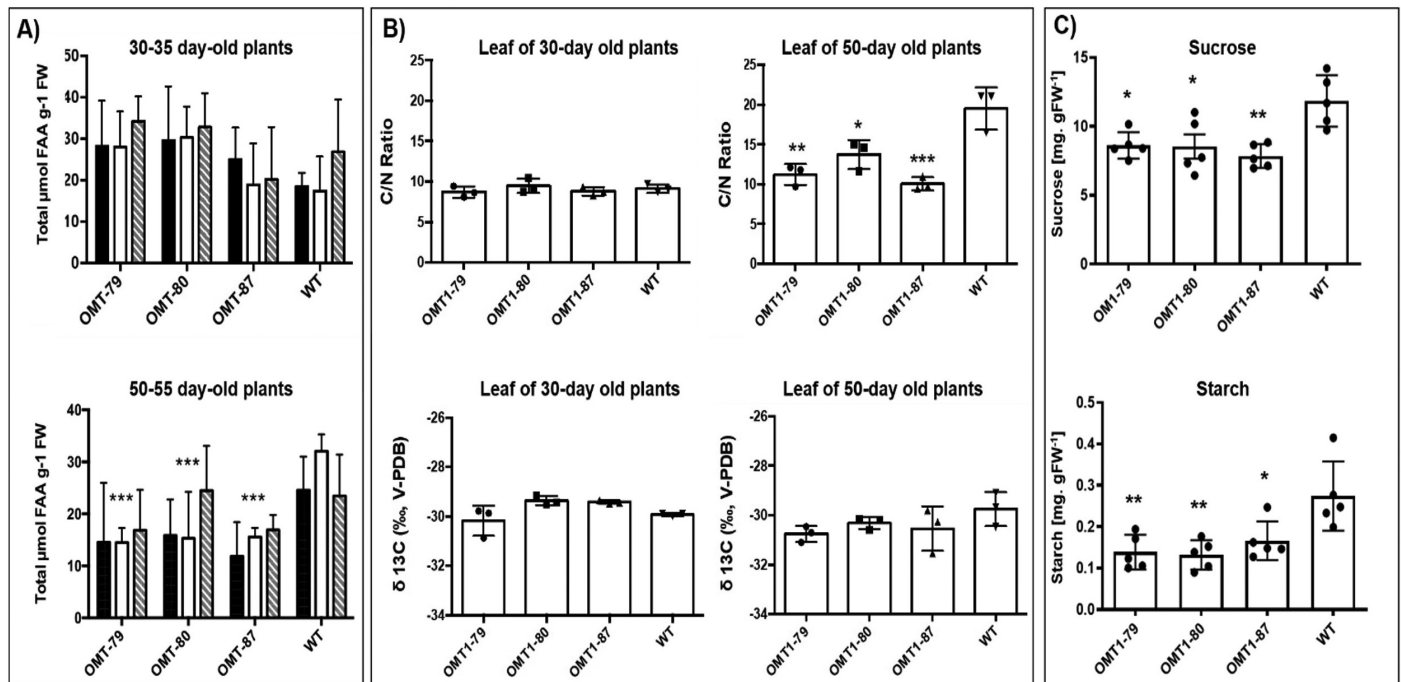


**Fig. 8.** Absolute amounts of total free amino acid (FAA) content (A), and the C:N ratio and $\delta^{13}C$ value (B) of OMT1 lines (OMT1-79, OMT1-80, and OMT1-87) and wild-type (WT) rice. (A) Samples collected under different $CO_2$ concentrations [$\mu$mol $CO_2$ $mol^{-1}$] (200, black; 400, white; and 1000, dashed pattern). Values represent the mean ±SEM, *n*=5. (B) Samples collected from 30- and 50-day-old OMT1 lines and WT rice. Values represent the mean ±SEM, *n*=3. Significant differences from the WT are indicated by *$P \leq 0.05$, **$P \leq 0.01$, and ***$P \leq 0$. 001, Tukey's multiple comparison test
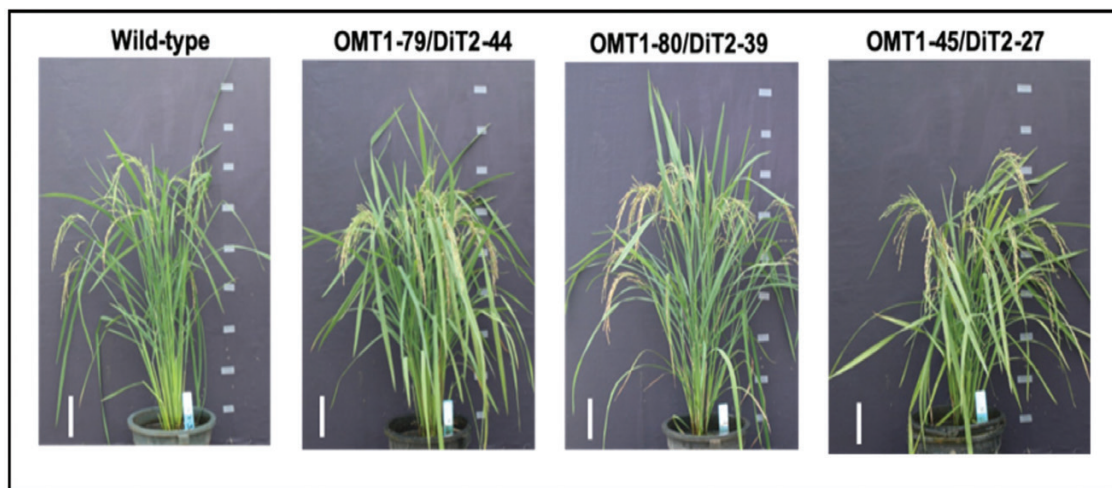


**Fig. 9.** Growth phenotype of the wild type and of double overexpressor lines OMT1-79/DiT2-44, OMT1-80/DiT2-39, and OMT1-45/DiT2-27. All plants were grown under ambient conditions; pictures were taken 90 d post-germination. Scale bar: 10 cm.
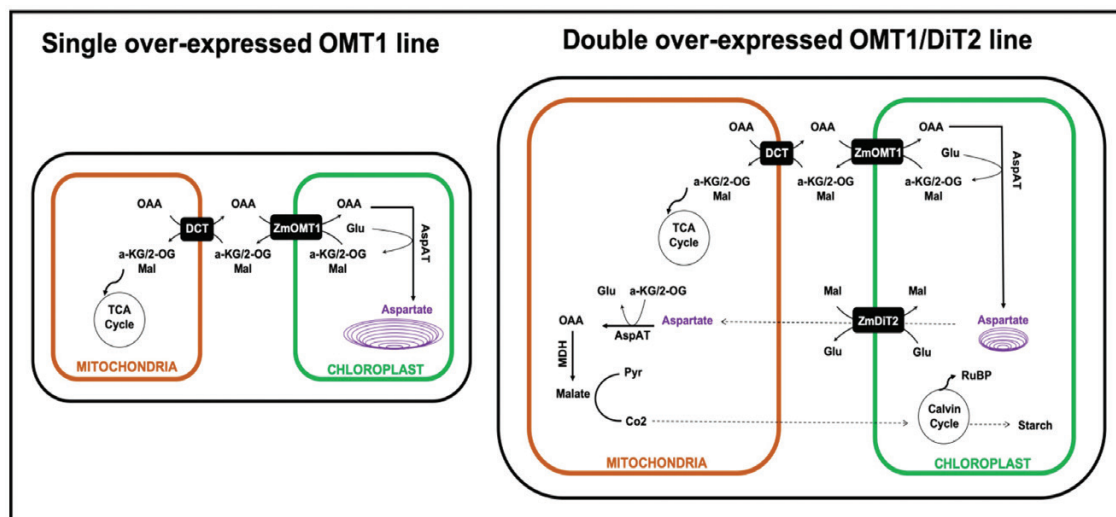
**Fig. 10.** Schematic of the metabolic scenarios in single OMT1 and double OMT1/DiT2 transgenic C$_3$ rice plants. We hypothesize that in single OMT1 overexpressing lines, OAA imported by OMT1 is converted to Asp, which is trapped inside the chloroplasts due to higher OMT1 than DiT2 activity. Overexpression of DiT1 in OMT1 lines rescues the phenotype by providing sufficient capacity for Asp export from chloroplasts.

**Table 3.** Leaf chlorophyll content, plant height, and tiller number of the wild type and OMT1/DiT2 double overexpressed lines

|                   | Chl (SPAD value) | Tiller number | Plant height (cm) |
|-------------------|------------------|---------------|-------------------|
| **Wild type**     | 43.8 ± 1.1 a     | 17.3 ± 1.6ns  | 99.3 ± 3.8 ab     |
| **OMT1-79/DiT2-44** | 39.9 ± 1.6 ab  | 24.7 ± 6.4ns  | 97.7 ± 1.8 a      |
| **OMT1-80/DiT2-39** | 40.9 ± 1.6 ab  | 13 ± 0.7ns    | 96.7 ± 3.1 ab     |
| **OMT1-45/DiT2-27** | 36.6 ± 1.5 b   | 18 ± 3.3ns    | 87.7 ± 4.7 b      |

Chlorophyll SPAD values are the average ±SEM of three leaves from three plants at mid-tillering stage using the upper fully expanded leaves. Tiller number and plant height are the average ±SEM of three individual F$_2$ plants at 90 d post-germination. Different letters within groups indicate that values are statistically different $P \leq 0.05$, Tukey's multiple comparison test. ns indicates non-significant, $P > 0.05$.

On the other hand, sucrose biosynthesis is occurring during the day (from the triose–phosphate pathway) and the night (from various enzymatic reactions involved in starch degradation) (Kunz *et al.*, 2014). Therefore, the metabolism of starch and sucrose tightly depend on each other, and both are orchestrated by the amount of the fixed carbon during photosynthesis. Taken together, apparently too high or too low amounts of OMT1 protein affect the coordination of the C and N assimilation pathways.

*Concluding model*

Our results present evidence on the crucial roles of the OMT1 transporter in rice plants. We suggest a hypothetical model (Fig. 10) in which aspartate accumulates in chloroplasts of single OMT1 transgenic lines in comparison with wild-type rice (Fig. 7D). We propose that the accumulated aspartate impairs the flux between the inside and outside of the chloroplast, causing the growth and photosynthetic deficiency phenotypes

in single OMT1 transgenic lines. Our assumption is supported by the finding that providing an exit pathway for aspartate by introducing an additional plastidial transporter (ZmDiT2) suppresses the phenotype of OMT1 overexpression (Fig. 10). These double overexpressor OMT1/DiT2 lines grew similarly to the wild type, and plant height along with numbers of tillers were recovered (Table 3). Our results indicate that coordinated expression of OMT1 and DiT2 is needed for engineering C$_4$ rice plants.

## Supplementary data

The following supplementary data are available at *JXB* online.

Fig. S1. Schematic of the pSC110:*ZmOMT1*:AcV5 construct.

Fig. S2. Representative pictures of wild-type, DiT2-44, DiT2-39 and DiT2-27 lines grown under ambient conditions; 80 d post-germination.

Fig. S3. DNA blots showing that the OMT1 lines (OMT1-79, OMT1-80, and OMT1-87) carry a single copy of the *ZmOMT1* CDS and are homozygous at the T$_3$ generation.

Fig. S4. Relative amount of some individual amino acids in OMT1 lines (OMT1-79, OMT1-80, and OMT1-87) and wild-type (WT) plants under different CO$_2$ concentrations (200, 400, and 1000 ppm).

Fig. S5. Western blot analysis of *Zm*OMT1 and *Zm*DiT2 protein expression in rice cross lines of OMT1/DiT2 (1, 2, 3, and 4).

Fig. S6. RT-PCR of *ZmOMT1* and *ZmDiT2* mRNA expression in OMT1/DiT2 double transgenic lines together with the wild type (WT).

Table S1. Primers used in this study.

Table S2. $V_{cmax}$ and $J_{max}$ based on $A/C_i$ data at 21% or 2% O$_2$ using the PsFit Model.

## Acknowledgements

## References

**Bai Z, Wang J, Wang M, Gao M, Sun J.** 2018. Accuracy assessment of multi-source gridded population distribution datasets in China. Sustainability **10**, 1363.

**Bernacchi CJ, Pimentel C, Long SP.** 2003. In vivo temperature response functions of parameters required to model RuBP-limited photosynthesis. Plant, Cell & Environment **26**, 1419–1430.

**Bernacchi CJ, Singsaas EL, Pimentel C, Portis AR Jr, Long SP.** 2001. Improved temperature response functions for models of Rubisco-limited photosynthesis. Plant, Cell & Environment **24**, 253–259.

**Breuers FKH, Bräutigam A, Geimer S, Welzel UY, Stefano G, Renna L, Brandizzi F, Weber APM.** 2012. Dynamic remodeling of the plastid envelope membranes—a tool for chloroplast envelope in vivo localizations. Frontiers in Plant Science **3**, 1–10.

**Edwards EJ, Osborne CP, Strömberg CA, *et al*.** 2010. The origins of C4 grasslands: integrating evolutionary and ecosystem science. Science **328**, 587–591.

**FAO.** 2017. The future of food and agriculture—trends and challenges. Rome: FAO www.fao.org/3/a-i6583e.pdf.

**Farquhar GD, von Caemmerer S, Berry JA.** 1980. A biochemical model of photosynthetic $CO_2$ assimilation in leaves of $C_3$ species. Planta **149**, 78–90.

**Fernie AR, Martinoia E.** 2009. Malate. Jack of all trades or master of a few? Phytochemistry **70**, 828–832.

**Fiehn O.** 2007. Validated high quality automated metabolome analysis of *Arabidopsis thaliana* leaf disks. In: Nikolau BJ, Wurtele ES, eds. Concepts in plant metabolomics. New York: Springer, 1–18.

**Forde BG, Lea PJ.** 2007. Glutamate in plants: metabolism, regulation, and signalling. Journal of Experimental Botany **58**, 2339–2358.

**Furbank RT, Scofield GN, Hirose T, Wang X-D, Patrick JW, Offler CE.** 2001. Cellular localisation and function of a sucrose transporter OsSUT1 developing rice grains. Australian Journal of Plant Physiology **28**, 1187–1196.

**Ghannoum O, Evans JR, Von Caemmerer S.** 2011. Nitrogen and water use efficiency of C4 plants. In: Raghavendra AS, Sage RF, eds. C4 photosynthesis and related $CO_2$ concentrating mechanisms. Dordrecht, The Netherlands: Springer, 129–146.

**Giuliani R, Koteyeva N, Voznesenskaya E, Evans MA, Cousins AB, Edwards GE.** 2013. Coordination of leaf photosynthesis, transpiration, and structural traits in rice and wild relatives (genus *Oryza*). Plant Physiology **162**, 1632–1651.

**Gracen VE Jr, Hilliard JH, Brown RH, West SH.** 1972*a*. Peripheral reticulum in chloroplasts of plants differing in $CO_2$ fixation pathways and photorespiration. Planta **107**, 189–204.

**Gracen VE, Hilliard JH, West SH.** 1972*b*. Presence of peripheral reticulum in chloroplasts of Calvin cycle cells. Journal of Ultrastructure Research **38**, 262–264.

**Guillemaut P, Maréchal-Drouard L.** 1992. Isolation of plant DNA: a fast, inexpensive, and reliable method. Plant Molecular Biology Reporter **10**, 60–65.

**Haferkamp I, Linka N.** 2012. Functional expression and characterization of membrane transport proteins. Plant Biology **14**, 675–690.

**Hibberd JM, Sheehy JE, Langdale JA.** 2008. Using C4 photosynthesis to increase the yield of rice—rationale and feasibility. Current Opinion in Plant Biology **11**, 228–231.

**Hilliard JH, West SH.** 1971. The association of chloroplast peripheral reticulum with low photorespiration rates in a photospiring plant species. Planta **99**, 352–356.

**Jain M, Nijhawan A, Tyagi AK, Khurana JP.** 2006. Validation of housekeeping genes as internal control for studying gene expression in rice by quantitative real-time PCR. Biochemical and Biophysical Research Communications **345**, 646–651.

**Khoshravesh R, Lundsgaard-Nielsen V, Sultmanis S, Sage TL.** 2017. Light microscopy, transmission electron microscopy, and immunohistochemistry protocols for studying photorespiration. Methods in Molecular Biology **1653**, 243–270.

**Kinoshita H, Nagasaki J, Yoshikawa N, Yamamoto A, Takito S, Kawasaki M, Sugiyama T, Miyake H, Weber APM, Taniguchi M.** 2011. The chloroplastic 2-oxoglutarate/malate transporter has dual function as the malate valve and in carbon/nitrogen metabolism. The Plant Journal **65**, 15–26.

**Kramer DM, Evans JR.** 2011. The importance of energy balance in improving photosynthetic productivity. Plant Physiology **155**, 70–78.

**Kromdijk J, Long SP.** 2016. One crop breeding cycle from starvation? How engineering crop photosynthesis for rising $CO_2$ and temperature could be one important route to alleviation. Proceedings of the Royal Society B: Biological Sciences **283**, 20152578.

**Kunz HH, Zamani-Nour S, Häusler RE, Ludewig K, Schroeder JI, Malinova I, Fettke J, Flügge UI, Gierth M.** 2014. Loss of cytosolic phosphoglucose isomerase affects carbohydrate metabolism in leaves and is essential for fertility of Arabidopsis. Plant Physiology **166**, 753–765.

**Laetsch WM.** 1968. Chloroplast specialization in dicotyledons possessing the $C_4$-dicarboxylic acid pathway of photosynthetic $CO_2$ fixation. American Journal of Botany **55**, 875–883.

**Laetsch WM.** 1969. Relationship between chloroplast structure and photosynthetic carbon fixation pathways. Science Progress Oxford **57**, 323–351.

**Laetsch WM.** 1974. The C4 syndrome: a structural analysis. Annual Review of Plant Physiology **25**, 27–52.

**Lin H, Karki S, Coe RA, *et al*.** 2016. Targeted knockdown of GDCH in rice leads to a photorespiratory-deficient phenotype useful as a building block for C4 rice. Plant & Cell Physiology **57**, 919–932.

**Mackill DJ, Khush GS.** 2018. IR64: a high-quality and high-yielding mega variety. Rice **11**, 18.

**Makino A, Osmond B.** 1991. Effects of nitrogen nutrition on nitrogen partitioning between chloroplasts and mitochondria in pea and wheat. Plant Physiology **96**, 355–362.

**Muthayya S, Sugimoto JD, Montgomery S, Maberly GF.** 2014. An overview of global rice production, supply, trade, and consumption. Annals of the New York Academy of Sciences **1324**, 7–14.

**Nunes-Nesi A, Fernie AR, Stitt M.** 2010. Metabolic and signaling aspects underpinning the regulation of plant carbon nitrogen interactions. Molecular Plant **3**, 973–996.

**Osborn HL, Alonso-Cantabrana H, Sharwood RE, Covshoff S, Evans JR, Furbank RT, von Caemmerer S.** 2017. Effects of reduced carbonic anhydrase activity on $CO_2$ assimilation rates in *Setaria viridis*: a transgenic analysis. Journal of Experimental Botany **68**, 299–310.

**Palmieri F, Indiveri C, Bisaccia F, Iacobazzi V.** 1995. Mitochondrial metabolite carrier proteins: purification, reconstitution, and transport studies. Methods in Enzymology **260**, 349–369.

**Pottosin I, Shabala S.** 2016. Transport across chloroplast membranes: optimizing photosynthesis for adverse environmental conditions. Molecular Plant **9**, 356–370.

**Roell MS, Kuhnert F, Zamani-Nour S, Weber APM.** 2017. In vitro analysis of metabolite transport proteins. Methods in Molecular Biology **1653**, 83–96.

**Rosado-Alberio J, Weier TE, Stocking CR.** 1968. Continuity of the chloroplast membrane systems in *Zea mays* L. Plant Physiology **43**, 1325–1331.

**Rottet S, Besagni C, Kessler F.** 2015. The role of plastoglobules in thylakoid lipid remodeling during plant development. Biochimica et Biophysica Acta **1847**, 889–899.

**Sage RF, Sage TL, Kocacinar F.** 2012. Photorespiration and the evolution of $C_4$ photosynthesis. Annual Review of Plant Biology **63**, 19–47.

**Sage TL, Sage RF.** 2009. The functional anatomy of rice leaves: implications for refixation of photorespiratory $CO_2$ and efforts to engineer $C_4$ photosynthesis into rice. Plant & Cell Physiology **50**, 756–772.

**Schneider CA, Rasband WS, Eliceiri KW.** 2012. NIH image to ImageJ: 25 years of image analysis. Nature Methods **9**, 671–675.

**Schneidereit J, Häusler RE, Fiene G, Kaiser WM, Weber AP.** 2006. Antisense repression reveals a crucial role of the plastidic 2-oxoglutarate/malate translocator DiT1 at the interface between carbon and nitrogen metabolism. The Plant Journal **45**, 206–224.

**Selinski J, Scheibe R.** 2019. Malate valves: old shuttles with new perspectives. Plant Biology **21** Suppl 1, 21–30.

**Shameer S, Ratcliffe RG, Sweetlove LJ.** 2019. Leaf energy balance requires mitochondrial respiration and export of chloroplast NADPH in the light. Plant Physiology **180**, 1947–1961.

**Simon P.** 2003. Q-Gene: processing quantitative real-time RT–PCR data. Bioinformatics **19**, 1439–1440.

**Smith AM, Agiza AH.** 1951. The determination of amino-acids colorimetrically by the ninhydrin reaction. The Analyst **76**, 623–627.

**Smith AM, Zeeman SC.** 2006. Quantification of starch in plant tissues. Nature Protocols **1**, 1342–1345.

**Stitt M, Zeeman SC.** 2012. Starch turnover: pathways, regulation and role in growth. Current Opinion in Plant Biology **15**, 282–292.

**Szczepanik J, Sowinski P.** 2014. The occurrence of chloroplast peripheral reticulum in grasses: a matter of phylogeny or a matter of function? Acta Physiologiae Plantarum **36**, 1133–1142.

**Taniguchi M, Miyake H.** 2012. Redox-shuttling between chloroplast and cytosol: integration of intra-chloroplast and extra-chloroplast metabolism. Current Opinion in Plant Biology **15**, 252–260.

**Taniguchi M, Taniguchi Y, Kawasaki M, Takeda S, Kato T, Sato S, Tabata S, Miyake H, Sugiyama T.** 2002. Identifying and characterizing plastidic 2-oxoglutarate/malate and dicarboxylate transporters in *Arabidopsis thaliana*. Plant & Cell Physiology **43**, 706–717.

**Tobin AK, Yamaya T.** 2001. Cellular compartmentation of ammonium assimilation in rice and barley. Journal of Experimental Botany **52**, 591–604.

**Udvardi MK, Czechowski T, Scheible WR.** 2008. Eleven golden rules of quantitative RT-PCR. The Plant Cell **20**, 1736–1737.

**van Wijk KJ, Kessler F.** 2017. Plastoglobuli: plastid microcompartments with integrated functions in metabolism, plastid developmental transitions, and environmental adaptation. Annual Review of Plant Biology **68**, 253–289.

**Walker BJ, Strand DD, Kramer DM, Cousins AB.** 2014. The response of cyclic electron flow around photosystem I to changes in photorespiration and nitrate assimilation. Plant Physiology **165**, 453–462.

**Wang P, Vlad D, Langdale JA.** 2016. Finding the genes to build $C_4$ rice. Current Opinion in Plant Biology **31**, 44–50.

**Weber A, Menzlaff E, Arbinger B, Gutensohn M, Eckerskorn C, Flügge UI.** 1995. The 2-oxoglutarate/malate translocator of chloroplast envelope membranes: molecular cloning of a transporter containing a 12-helix motif and expression of the functional protein in yeast cells. Biochemistry **34**, 2621–2627.

**Yin X, Anand A, Quick WP, Bandyopadhyay A.** 2019. Editing a stomatal developmental gene in rice with CRISPR/Cpf1. Methods in Molecular Biology **1917**, 257–268.

**Yoshida S, Forno DA, Cock JH, Gomez KA.** 1972. Routine procedure for growing rice plants in culture solution. In: Yoshida S, Forno DA, Cock JH, eds. Laboratory manual for physiological studies of rice. Los Baños, Philippines: International Rice Research Institute, 61–66.